Journal of Magnetism and Magnetic Materials 322 (2010) 633–637

Contents lists available at ScienceDirect

Journal of Magnetism and Magnetic Materials

journal homepage: www.elsevier.com/locate/jmmm

Magnetic composites based on hybrid spheres of aluminum oxide and superparamagnetic nanoparticles of iron oxides

Tiago P. Braga [a], Igor F. Vasconcelos [b], José M. Sasaki [c], J.D. Fabris [d], Diana Q.L. de Oliveira [d], Antoninho Valentini [a,*]

[a] Langmuir – Laboratório de Adsorção e Catálise, Departamento de Química Analítica e Físico-Química, Universidade Federal do Ceará, CP 6021, CEP 60455-970 Campus do Pici, Fortaleza, Brazil
[b] Departamento de Engenharia Metalúrgica e de Materiais, Universidade Federal do Ceará, Fortaleza, Brazil
[c] Laboratório de Raios X, Departamento de Física, Universidade Federal do Ceará, Campus do Pici, Fortaleza, CE, Brazil
[d] Departamento de Química, Universidade Federal de Minas Gerais, Belo Horizonte, Brazil

ARTICLE INFO

Article history:
Received 15 July 2009
Received in revised form
8 October 2009
Available online 29 October 2009

Keywords:
Hybrid sphere
Nanoparticle
Iron oxide
Aluminum
Superparamagnetic

ABSTRACT

Materials containing hybrid spheres of aluminum oxide and superparamagnetic nanoparticles of iron oxides were obtained from a chemical precursor prepared by admixing chitosan and iron and aluminum hydroxides. The oxides were first characterized with scanning electron microscopy, X-ray diffraction, and Mössbauer spectroscopy. Scanning electron microscopy micrographs showed the size distribution of the resulting spheres to be highly homogeneous. The occurrence of nano-composites containing aluminum oxides and iron oxides was confirmed from powder X-ray diffraction patterns; except for the sample with no aluminum, the superparamagnetic relaxation due to iron oxide particles were observed from Mössbauer spectra obtained at 298 and 110 K; the onset six line-spectrum collected at 20 K indicates a magnetic ordering related to the blocking relaxation effect for significant portion of small spheres in the sample with a molar ratio Al:Fe of 2:1.
© 2009 Elsevier B.V. All rights reserved.

1. Introduction

Composite materials containing iron oxides are widely used in technologies of gas sensors [1], magnetic refrigeration [2], data storage in computer devices [3], adsorbents [4], and chemical catalysts [5]. Developing an efficient and sufficiently practical methodology to prepare such composites, as those based on magnetic iron oxides, has been a matter of many relatively recent research works, particularly those involving sol–gel method [6], electrochemical techniques [7], chemical vapor deposition [8], or pyrolysis [9].

Nanoscaled materials present unique physical and chemical features, comparatively to their bulk form, making them of particular interests from scientific and technological viewpoints. Nanoparticles with magnetic properties have potential applications in several more specific areas of either *in vivo* or *in vitro* biological researches on modern medical practices [10,11]. To gain practical uses, such small magnetic particles must have high saturation magnetization (M_S) and coercivity (H_C) [12]. Bulk metallic iron itself does present such a required high saturation but its coercivity is in practice rather low. On the other hand, the coercivity magnitude of metallic iron nanoparticles is significantly higher than the corresponding coarser, bulk material [13]. Superparamagnetic effects are somehow directly related to the exceptionally small size of magnetic nanoparticles, since particles with diameters below a given threshold values usually are recognized to exhibit these characteristics[14]. As a result of this, materials with superparamagnetic behavior have been extensively used in biomedical practices[15,16]. Previously reported results in the scientific literature have dealt with applications of nanoparticles of magnetic iron oxide to separate biochemical products or cells [17], to clinically treat cancer tumors [18].

The applicability and efficiency of a nanoparticulated material also depend upon particles uniformity both in size and in shape. Even though different shapes eventually represent, in some cases, particular advantages, spherical shape would be conceptually preferable, taking into their relatively higher surface area to volume ratio. The ability to control size and morphology of nanoparticles may determine the preparation of tailored materials destined to these specific applications [19].

In this work, we report results on the preparation of hybrid spheres, containing nanosized aluminum and iron oxide, obtained from a synthesis route starting on an organic substrate precursor. The synthesized material was characterized with scanning electron microscopy, X-ray diffraction, and Mössbauer spectroscopy.

2. Experimental procedures

Samples of hybrid spheres of aluminum oxide and iron oxide were obtained *via* a method employing chitosan, a polysaccharide

* Corresponding author.
E-mail address: valent@ufc.br (A. Valentini).

0304-8853/$ - see front matter © 2009 Elsevier B.V. All rights reserved.
doi:10.1016/j.jmmm.2009.10.028

derived from D-glucosamine, as an organic precursor, and aluminum and iron salts: 5.5 g of chitosan was dissolved in 300 mL of CH_3COOH solution (5% v/v); separately, 26.98 g of $Al(NO_3)_3 \cdot 9H_2O$ and 4.85 g of $Fe(NO_3)_3 \cdot 9H_2O$ were dissolved in 100 mL of water. The iron + aluminum aqueous solution was poured into the chitosan solution, under constant stirring. The resulting solution, from now on to be referred to as simply Fe–Al–chitosan solution, was drop wise pumped into a NH_4OH aqueous solution (30% v/v), under stirring, with a peristaltic pump. The gel spheres so formed were separated from the NH_4OH solution medium and dried at room temperature for 96 h. The dried samples were calcined in airflow, during 1 h at 500 °C, under a heating rate of 5 °C min^{-1}. During the polymeric precursor elimination process, the iron and/or aluminum oxide spheres were formed. The Fe–Al–chitosan solutions were prepared with a ratio of 2.5 ions (Fe and Al) to each monomer of chitosan. Samples with different Al to Fe molar ratios were prepared and labeled AlFe*X*, where *X* denotes the Al:Fe molar ratio. The sample labeled Al contained only aluminum oxide.

The morphology and mean diameter of spheres were examined with a Philips XL30 scanning electron microscope (SEM), operating with an accelerating voltage of 20 kV. The X-ray diffraction (XRD) analysis was performed in a Rigaku-DMAXB X-ray diffractometer using Bragg–Brentano geometry in the range of 10–80° with a rate of 0.5 °min^{-1}. CuKα radiation (λ=1.5405 Å) was used and the tube operated at 40 kV and 25 mA. The phase identification analysis was made by comparing obtained powder diffractograms with standard patterns from International Centre for Diffraction Data (ICDD). For the sample AlFe0, the experimental patterns were numerically fitted with the Rietveld algorithm [20] in a procedure to better identify and quantify crystallographic phases. Mean nanoparticles sizes, when applied, were estimated by using the Scherrer's equation [21]. Transmission Mössbauer spectra were recorded at room temperature, 110 K, and at 20 K, in constant acceleration mode setup, with a ^{57}Co (Rh) source. The Mössbauer data were fitted to discrete Lorentzian functions, using the least-square fitting routine of the NORMOS® software package. All isomer shift values (δ) are quoted relatively to αFe.

3. Results and discussion

Fig. 1 illustrates the hybrid spheres immediately after being separated from the aqueous solution of ammonia. The average diameter of spheres, determined at this stage, is 3.08 mm with standard deviation of 0.34; this mean value was determined considering a total of 350 spheres. Therefore, a reasonably uniformity of sizes throughout the entire sample mass is confirmed from the image (Fig. 1). After the drying process, the mean diameter of spheres is significantly reduced, as it can also be observed from SEM micrographs (Fig. 2), indicating that volumes of individual sphere are significantly influenced by water retained by particles during the chemical synthesis. After drying at room temperature, the mean diameters for samples $AlFe_6$ and $AlFe_0$ were found to be 1.42 and 1.69 mm, respectively. After calcination at 500°C under airflow, the mean diameters for samples $AlFe_6$ and $AlFe_0$ became 1.02 and 1.53 mm, respectively (Fig. 2a and c). The occurrence of some particles surface cracked (Fig. 2b and d) points to the need of improving further the mechanical resistance of the material. However, this is an issue being addressed in a future report, as corresponding data are still being more accurately collected.

The calcinated samples were also analyzed with X-ray diffraction; results are presented in Fig. 3. All patterns, except for sample AlFe0, present broad peaks, indicating that crystallites

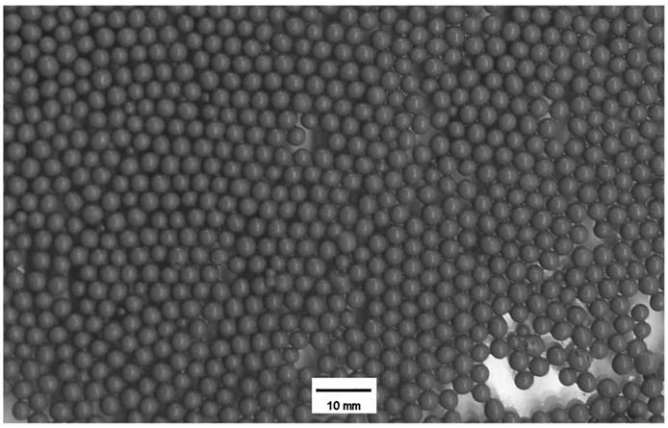

Fig. 1. Spheres immediately after the preparation process (AlFe6).

are rather small. Two crystalline phases of iron oxide were identified from the diffraction profile of sample AlFe0 (see Fig. 3b): αFe_2O_3 (hematite, JCPDS card # 87-1166) and γFe_2O_3 (maghemite, JCPDS card # 25-1402). Table 1 shows proportions of the main occurring phases.

The diffraction patterns for samples AlFe15, AlFe6, and Al (Fig. 3a) show the occurrence of Al_2O_3 (JCPDS card # 10-0425); figures for sample AlFe6 and AlFe2 reveal also the co-existence of iron oxide phases, namely αFe_2O_3 (hematite, JCPDS card # 87-1166) and γFe_2O_3 (maghemite, JCPDS card # 25-1402). Reflections associated with Al-bearing phases were not readily identified from the pattern for sample AlFe2, whereas Fe-bearing phases were not identified in the pattern for sample AlFe15. This is not unexpected as samples AlFe2 and AlFe15 have, respectively, the highest and lowest Fe:Al ratios of all samples containing simultaneously the two elements. These results suggest that the high aluminum ratio inhibits the formation of iron-containing compounds, such as hematite or magnetite, and are consistent with other reportedly results [22,23]. This influence may be explained in terms of the ionic radii of the elements as the radius of octahedral Al^{3+} (0.53 Å) is comparable to that of Fe^{3+} (0.67 Å). Similar ionic radii favor the insertion of isomorphic Al^{3+} into the structure of iron oxide, but this replacement tends to inhibit the hematite crystallization.

Any attempt to perform the Rietveld refinement of XRD data for samples Al, AlFe15, AlFe6, and AlFe2 did not yield reliable results as samples are poorly crystalline. The average crystallite diameter of the different phases as estimated with the Scherrer's formula [21] is shown in Table 1. The mean coherent lengths (MCL) for Al_2O_3 in samples Al, AlFe15, and AlFe6 were found to be, respectively, 2.0, 2.0, and 2.9 nm; for αFe_2O_3 in samples AlFe6 and AlFe2, 2.8 and 3.0 nm in diameter; for γFe_2O_3, 2.6 and 2.5 nm. MCL values for αFe_2O_3 and γFe_2O_3 in the more crystalline AlFe0 were found as being 9.9 and 9.0 nm. Data in Table 1 suggest that the increasing content of aluminum oxide tends to decrease in the diameter of iron oxide crystallites.

The local environment of iron atoms in the iron-containing samples was investigated by Mössbauer spectroscopy. Fig. 4 shows the fitted spectra; the corresponding hyperfine parameters are presented in Table 2. The room temperature spectra obtained for samples AlFe15, AlFe6, and AlFe2 (Fig. 4a) show similar features with a central doublet suggesting that iron is in a (super) paramagnetic state. The Mössbauer signal for sample AlFe15 corroborates the assumption that Fe-based phases are not identifiable by XRD due to low Fe:Al ratio and to the extremely small particle sizes.

XRD analysis confirms the existence of very fine-grained αFe_2O_3 and γFe_2O_3 (Table 1) in all samples, whereas the doublets

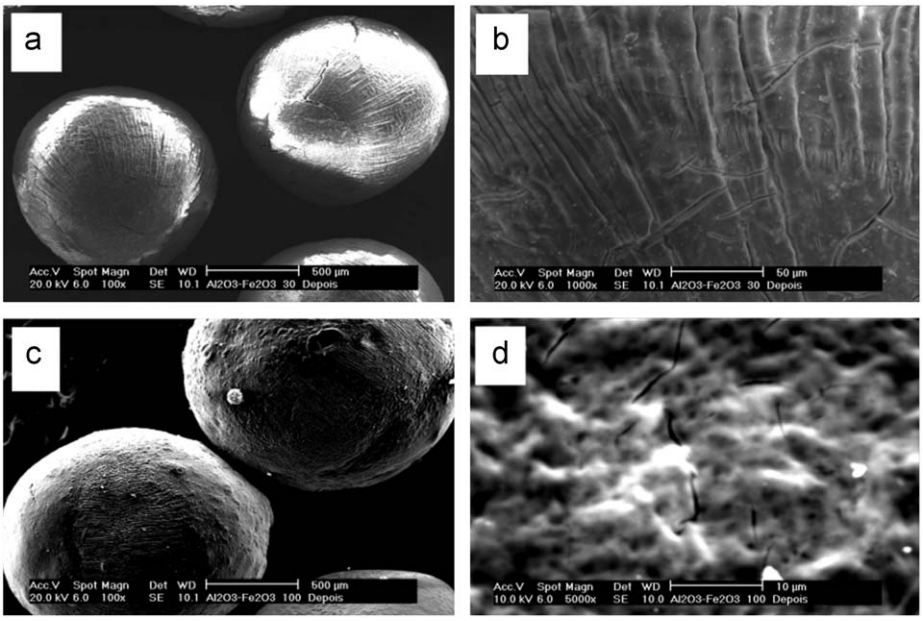

Fig. 2. SEM images of spheres: (a, b) AlFe6 sample after calcination, magnified by 100 and 1000 times, respectively. (c, d) AlFe0 sample after calcination, magnified by 100 and 5000 times, respectively.

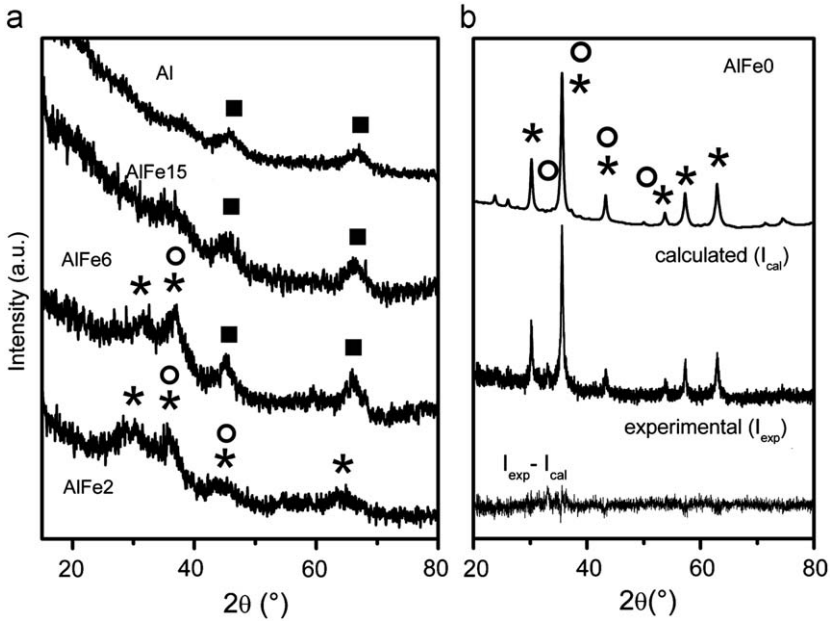

Fig. 3. X-ray powder diffraction of the spheres after calcination at 500°C: (a) Samples containing Al, and (b) AlFe0 sample. (■) Al_2O_3 phase, (○) αFe_2O_3 phase, (*) γFe_2O_3 phase, according to the standard diffractions.

Table 1
Relative mass percentage of the phases observed and grain size.

Sample	Mass of crystalline phase (%)			Grain size (nm)		
	Al_2O_3	αFe_2O_3	γFe_2O_3	Al_2O_3	αFe_2O_3	γFe_2O_3
Al	100.0	–	–	2.0	–	–
AlFe15	100.0	–	–	2.0	–	–
AlFe6	–	–	–	2.9	2.8	2.6
AlFe2	–	–	–	–	3.0	2.5
AlFe0	–	10.0	90.0	–	9.9	9.0

observed in the Mössbauer spectra confirm that the iron phases in samples AlFe15, AlFe6, and AlFe2 are in a superparamagnetic state. When particle sizes are smaller than a critical threshold, the superparamagnetic relaxation phenomenon occurs [24,25]. These observations are consistent with results recently published [26–28].

Mössbauer spectra (Fig. 4b) for sample AlFe2 taken at low temperatures confirm its superparamagnetic state. Corresponding hyperfine parameters are shown in Table 2. While at 110 K the sample still remains superparamagnetic, at 20 K a great deal of magnetic moments is blocked as it is evidenced by the appearance of a broad and asymmetric magnetic sextet. The remaining central doublet may suggest that moments are only partially blocked even at 20 K. The blocking temperature is a function of particle size. In this case, the mean diameters for aluminum-containing samples are in the range of 2.0 and ~3.0 nm (Table 1). The sample AlFe0, on the other hand, presents particles larger than those in

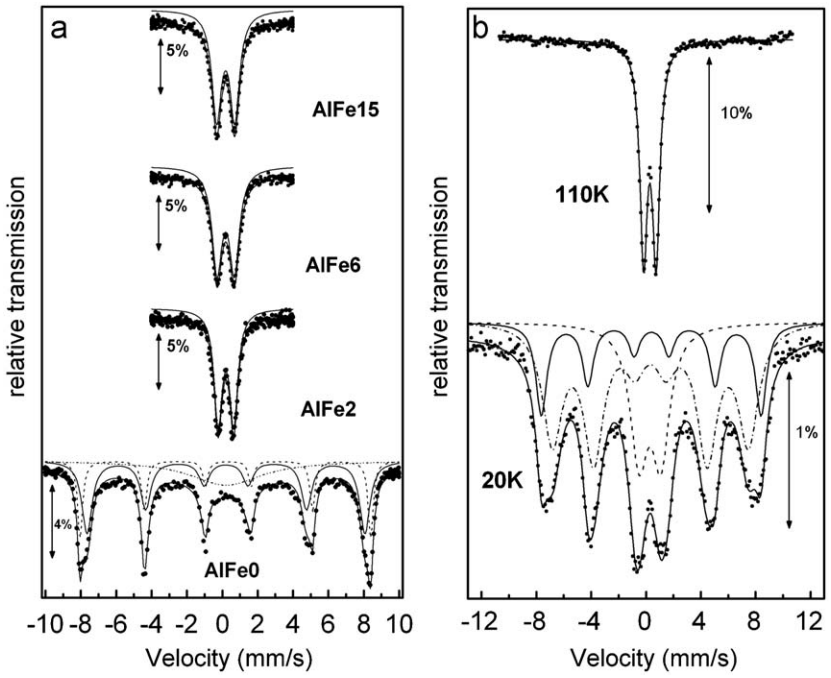

Fig. 4. 57Fe Mössbauer spectra for (a) the samples containing iron oxide, at room temperature, and (b) the sample AlFe2 at 110 and 20 K.

Table 2
^{57}Fe Mössbauer hyperfine parameters for samples containing iron.

Sample	Temperature (K)	δ (mm s^{-1}) ($\pm$0.05)	Δ or ε (mm s^{-1}) ($\pm$0.05)	B_{hf} (T) ($\pm$0.5)	*RA* (%) ($\pm$1)
AlFe15	300	0.30	1.02		100
AlFe6	300	0.30	0.98		100
AlFe2	300	0.32	0.91		100
AlFe0	300	0.37	−0.17	50.93	25
		0.32	~0	49.71	46
					28
AlFe2	110	0.39	0.91		100
AlFe2	20	0.39	1.59		22
		0.50	0.03	49.7	20
		0.43	0.01	44.3	58

δ: isomer shift relative do αFe; Δ: quadrupole splitting; ε: quadrupole shift; B_{hf}: hypefine field and *RA*: relative subspectral area.

the other samples and thus two six line-subspectra are observed in the corresponding Mössbauer spectrum at room temperature (Fig. 4a). One of them, with isomer shift relative to αFe δ=0.32 mm s^{-1}, quadrupole shift ε=−0.17 mm s^{-1}, and magnetic hyperfine field B_{hf}=50.93 T (Table 2) is assignable to hematite, while the other, with δ=0.32 mm s^{-1}, ε~0 mm s^{-1}, and B_{hf}=49.71 T, is due to maghemite, according to typical reported values for these iron oxides [29,30].

4. Conclusions

A simple method employing an organic precursor and metallic salts was used to prepare nanoparticles of aluminum oxide and of superparamagnetic iron oxides, and prepare composites with different iron:aluminum ratios, and relatively uniform spherical shapes and sizes. X-ray diffraction measurements confirmed the presence of fine-grained alumina, hematite, and maghemite all samples. Aluminum-bearing phases were not identified in the sample with the smallest aluminum:iron ratio, whereas iron oxides were not readily identified in the sample with the smallest iron:aluminum ratio. The doublet existence in the Mössbauer spectrum of the latter corroborates the assumption that Fe-based phases are not identifiable by XRD due for the smallest Fe:Al ratio due to extremely fined particle size. Room temperature Mössbauer spectra for the composites containing Fe and Al oxides presented (super)paramagnetic doublets rather than the expected sextets for bulk hematite or maghemite, suggesting that iron-bearing phases in these samples are actually in a superparamagnetic state, as sizes of particles are smaller than a critical threshold value. This assumption is confirmed by the Mössbauer measurement at 20 K, for which a great deal of blocked magnetic moments occurs, as evidenced by the appearance of magnetic sextets for magnetically ordered species. The sample with no aluminum in its composition contains particles with sizes above the critical value and thus two six-lined subspectra associated to hematite and maghemite are observed in its Mössbauer spectrum at room temperature.

Acknowledgments

This work was financially supported by CNPq/CT-PETRO, CNPq, and FAPEMIG (Brazil). CNPq also granted a scholarship to T.P. Braga. Authors are also particularly grateful to Dr. José Domingos Ardisson (Research Center for the Development of Nuclear Technology, of the Brazilian National Commission on Nuclear Energy, Belo Horizonte, Minas Gerais, Brazil) for the Mössbauer measurement at 20 K.

References

[1] L.N. Geng, S.H. Wu, Mater. Chem. Phys. 99 (2006) 15.
[2] R.D. McMichael, R.E. Watson, J. Magn. Magn. Mater. 111 (1992) 29.
[3] M.P. Pileni, J. Phys. Chem. B 105 (2001) 3358.
[4] J. Youngran, M. Fan, J.V. Leeuwen, J.F. Belczyk, J. Environ. Sci 19 (2007) 910.
[5] A.C. Oliveira, M.C. Rangel, Catal. Today 85 (2003) 49.
[6] G. Ennas, G. Spano, Chem. Mater. 10 (1998) 495.
[7] C. Pascal, J.C. Payer, Chem. Mater. 11 (1999) 141.
[8] H.R. Orthner, P. Roth, Mater. Chem. Phys. 78 (2002) 453.

[9] S. Veintemillas-Verdaguer, C.J. Serna, Mater. Lett. 35 (1998) 227.
[10] C.M. Niemeyer, Angew. Chem. Int. 40 (2001) 4128.
[11] M.W. Freeman, A. Arrot, H.H.L. Watson, J. Appl. Phys. 31 (1960) 404.
[12] M. Pardavi-Horvath, et al., IEEE Trans. Magn. 28 (1992) 3186.
[13] W.H. Meiklejohn, Rev. Mod. Phys. 25 (1953) 302.
[14] Q. Chen, et al., J. Magn. Magn. Mater. 194 (1999) 1.
[15] R.A. Whitehead et al. US Patent 4,695,392, 1987.
[16] M. Shinkai, J. Biosci. Bioeng. 94 (2002) 606.
[17] P. Tartaj, et al., J. Phys. D Appl. Phys 36 (2003) 182.
[18] B. Ben-Nissan, MRS Bull. (2004) 28.
[19] I. Safarik, et al., J. Appl. Bacteriol. 78 (1995) 575.
[20] H.M. Rietveld, J. Appl. Crystallogr 2 (1967) 65.
[21] L.V. Azaroff, in: Elements of X-ray Crystallography, McGraw-Hill Book Company, New York, 1968.
[22] M. Liu, H. Li, L. Xiao, W. Yu, Y. Lu, Z. Zhao, J. Magn. Magn. Mater. 294 (2005) 294.
[23] Y.B. Pithawalla, M.S. El Shall, S.C. Deevi, Intermetallics 8 (2000) 1225.
[24] M. Steen, J. Magn. Magn. Mater 39 (1983) 45.
[25] M. Steen, Polyteknisk Forlag, Denmark, 1981, 260 pp.
[26] Z. Huang, F. Tang, L. Zhang, Thin Solid Films 471 (2005) 105.
[27] Z. Huang, F. TangJ. Colloid Interface Sci. 275 (2004) 142.
[28] Y.G. Maa, et al., Mater. Chem. Phys. 65 (2000) 79.
[29] M. Gotic, G. Koscec, S. Music, J. Molec. Struct. 924 (2008) 347.
[30] I. Mitov, D. Paneva, B. Kunev, Thermochim. Acta 386 (2002) 179.